We are IntechOpen, the world's leading publisher of Open Access books Built by scientists, for scientists

4,800
Open access books available

122,000
International authors and editors

135M
Downloads

Our authors are among the

154
Countries delivered to

TOP 1%
most cited scientists

12.2%
Contributors from top 500 universities

CLARIVATE ANALYTICS BOOK CITATION INDEX INDEXED

WEB OF SCIENCE™

Selection of our books indexed in the Book Citation Index in Web of Science™ Core Collection (BKCI)

Interested in publishing with us?
Contact book.department@intechopen.com

Numbers displayed above are based on latest data collected.
For more information visit www.intechopen.com

11

Atomic Force Microscopy – For Investigating Surface Treatment of Textile Fibers

Nemeshwaree Behary and Anne Perwuelz
ENSAIT-GEMTEX : ENSAIT, GEMTEX, Roubaix
Univ Lille Nord de France, USTL, F-59655, Villeneuve d'Ascq Cedex
France

1. Introduction

Textile fibers either natural or man-made (biodegradable and/or non biodegradable) are being increasingly used in non-traditional sectors such as technical textiles (automotive applications), medical textiles (e.g., implants, hygiene materials), geotextiles (reinforcement of embankments), agrotextiles (textiles for crop protection), and protective clothing (e.g., heat and radiation protection for fire fighter, bulletproof vests, and spacesuits).Textile structures (roving, knitted, woven or non woven) are also being increasingly used in textile reinforced composites.

Surface treatments of textile fibers, yarns or fabrics play an important role in their processing and end-use. The AFM-Atomic Force Microscopy seems a very valuable tool for investigating the effect of different fiber surface treatments and their impact on the final textile material properties. The AFM probe has been used to understand the frictional behaviour of sized glass fibers, and to study the impact of an air-atmospheric plasma treatment on polyethylene terephthalate fabrics

PART I: Use of AFM/LFM tool for friction analysis of sized glass fibers

1. Introduction

Glass fibers, generally used to reinforce composite materials, readily suffer abrasion damage due to friction when glass filaments slide against each other. In manufacturing, glass fibers are coated with a size consisting of a coupling agent, a lubricant, a film former and other additives. While the coupling agent is used to increase adhesion between the fibers and the matrix, in glass fiber reinforced composite materials (P.Plueddeman, 1982), the complete size should improve the frictional performance of contacting fibers surfaces during their processing and their uses (e.g.: spinning, weaving...). With the increasing demand for good sizing agents which have low friction values, it is important to study the frictional behavior of sized fibers.

1.1 Theoretical background of frictional properties of fibers

The frictional properties of polymer fibers deviate from the classical Amonton law. For polymers and fibers which are viscoelastic materials, the friction coefficient 'μ' depends on

the temperature, speed, and more specifically on the applied load. The most striking characteristic is that the coefficient of friction 'μ' increases as the load 'N' is diminished, and at light loads, it can be very high. Indeed, other than deformation at asperities observed in the fiber, the radius of curvature of the fiber surface is an important parameter in determining friction. Gupta described the friction of fibers in empirical terms (Gupta, 1992):

$$F_f = aN^n \quad (1)$$

with

$$\mu = aN^{n-1} \quad (2)$$

where 'a' and 'n' are constants, and $0<n<1$.

The friction coefficient 'μ' reaches its maximum value at zero load where the friction forces due to adhesive forces are present. In order to initiate motion during sliding, a certain force called static friction force 'F_s' must be applied, which is greater than the kinetic friction force 'F_k' needed to maintain the sliding. This may result in stick-slip motion when one fiber slides on another one, and this intermittent motion can be generated even in the presence of the size (Gupta, 1985, 1992). Friction force is reported to be at its highest at the stick phase (Israelachvili, 1993).

1.2 Static friction force and its relation to surface contact area and surface forces

It is generally accepted that static friction depends on adhesion forces, and recently Israelachvili (Israelachvili, 1993) has demonstrated that the frictional energy required during the static phase is used partly to overcome adhesion and partly to overcome the load. At very small loads, as in our case (nanonewtons for the LFM and micronewtons for the microbalance), the influence of load is small but adhesion forces (F_{ad}) are present. These forces depend on surface energy and on the apparent contact area. Surface energies are defined constants of materials, while the theoretical contact areas can be determined by contact mechanics theories. The first contact theory elaborated by Hertz concerns elastic solids for which the contact area for two contacting spheres, is a circle of radius 'a'. However in presence of adhesive forces, the contact areas may be altered and the two contact mechanics theories JKR (Johnson-Kendall-Roberts) (Johnson, 1971) and DMT (Derjaguin-Muller-Toporov) (Derjaguin, 1975) determine the real surface of contact.

The nature of fiber friction is known to be complex, and adequate theory describing it, is not available, though models have been provided to explain frictional behavior of fibrous materials (Gupta, 1992, 1993). The aim of this work was to use lateral force microscopy to investigate friction at nanoscale level and to relate the results to those obtained at a higher scale that is, during fiber-fiber friction, using an electronic microbalance.

2. Experimental

2.1 Friction force measurements by Lateral force microscopy

The atomic force microscopy/lateral force microscopy (AFM/LFM) invented by Bining & al. in 1986 (Binning, 1986) was used to obtain topographic image in the AFM mode, and lateral forces between a Si_3N_4 tip and a fiber surface in the LFM (lateral force microscopy) mode

(Meyer and Amer, 1990). Extensive reviews give detailed description of this apparatus and therefore only a brief explanation of the method will be described in this paper.

AFM imaging was achieved in air under atmospheric conditions with a commercial scanning probe «Nanoscope III, from Digital inc.», in the contact mode at a constant force. The AFM measures the vertical deflection of a cantilever to which is fixed a microtip which scans the sample surface (see Fig. 1). In the contact mode, the normal deflection (due to intermolecular forces) of the cantilever is dependent on the distance between the tip and the sample, such that $F_z = k.\ z$, where : F_z= deflection force of the cantilever, k= spring constant of the cantilever, and z= the cantilever's deflection.

The fiber sample is placed onto a piezodrive, while the tip is in a fixed position. The normal deflection of the cantilever is monitored through the displacement of a laser beam reflected off the cantilever onto a segmented detector, during the scanning of the sample in x and y directions (Fig. 1). Any bending of the cantilever due to bumps or grooves on the sample surface induces an intensity difference between the lower and upper part of the segmented photodetector, and this in turn provides an error signal for the feedback of the piezo so as to maintain a constant preset force on the cantilever. The displacement of the piezodrive allows the reconstitution of a topographic image of the scanned surface. The lateral force images were obtained by measuring the torque imposed on the cantilever by the tip as a result of tangential forces experienced by the tip, when the sample is moved underneath. To measure normal and lateral forces simultaneously a four quadrant photodiode is used (Fig. 1). The normal bending of the cantilever is measured by the intensity difference $(I_{1+2} - I_{3+4})$ of the upper and lower segments of the diode, while the signal difference of the left and the right segments $(I_{1+3} - I_{2+4})$ provides torsional information.

2.1.2 Topographical and LFM images

Topographical 3-dimensional as well as scope mode images were obtained in the AFM and LFM modes. Scope mode images give trace and retrace profiles of the topography and of LFM signals in real time when the sample goes forward and backward underneath the tip (see Fig. 2). Lateral force signals are influenced by the surface topography (slopes of a surface feature for example). For a surface with friction as well as with corrugations (see Fig. 2A and B), like the glass fibers used in this study, the normal reacting force (N) as well the frictional force (F_f) will have nonzero x, y, and z components, that is,

$$N = N_x + N_y + N_z$$

$$F_f = F_{fx} + F_{fy} + F_{fz}$$

In other words, the measured lateral force depends on the local slope as well and not only on frictional forces. The frictional force (F_f) is, of course, tangent to the slope (see Fig. 2B) and acts in the opposite direction to the scan direction, and, therefore, by the reversal of the scan direction, each of the components of the frictional force (F_f) changes sign, while those due to the normal force do not. The difference between the forward and the reverse scans in the LFM scope mode gives twice the average friction force (Overney and Meyer, 1993) Baselt and Baldeschwielder, 1992). Full quantification of the frictional force is not yet possible, so scanning was carried out 90° (Fig. 1) to cancel the y and z components of the friction force. Friction forces in volts were converted to Newtons by determining the lateral sensibility of

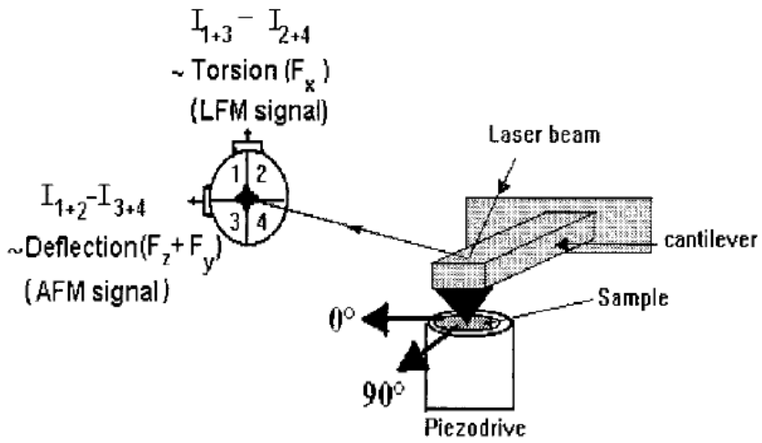

Fig. 1. Principle of simultaneous measurement of the normal and lateral forces; two scanning directions are possible (0° and 90°).

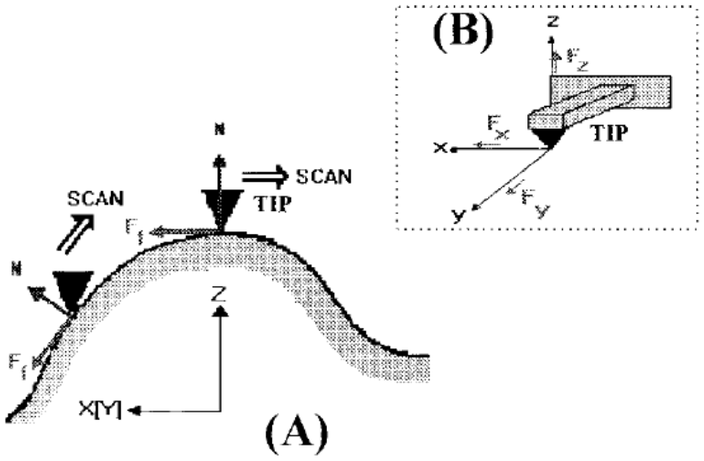

Fig. 2. (A) Normal reacting force (N) as well frictional force (F_f) acting on a surface with corrugations; (B) schematic presentation of the X, Y, and Z components of the forces acting at the top of the cantilever

the apparatus which was found to be 40 nN/V. Friction coefficients were obtained by dividing the friction force by the normal applied force.

2.1.3 Sample preparation

Sized glass filaments were provided by Owens Corning in the form of multifilament rovings. One or several of the filaments which are cylindrical in shape, were fixed onto a double-face Scotch tape, perpendicularly to the scan direction (90°), so as to measure both topographical and frictional data. This perpendicular position enables one to see in the scope mode the exact position of the fiber with respect to the tip point. As the maximum of the piezodrive in the *z* direction is limited to 5.9 µm, the fiber cannot be scanned wholly. So, only the most elevated part of the fiber, where the slope (or curvature) is minimum, was rastered. We shifted from a 6 x 6 to a 3 x 3µm² surface by zooming the top of the fiber, in the image mode, in real-time.

Samples were rastered at a constant force between 20 and 90 nN using a "J" head with scan area of 130 x 130 µm2 and conical-shaped ultralevers made from silicon nitride attached to the cantilever (180 µm long) with a spring constant k = 0.06 N/m. Topographic and lateral force images were obtained at a scan rate of 1.12 Hz with 512 samples per area scanned.

2.2 Fiber-Fiber friction force measurements using an electronic microbalance

An experimental device was set up using an electronic microbalance to measure fiber-fiber friction. An electronic microbalance having a sensitivity of 10^{-8} N was used since friction forces measured for two monofilaments of diameter 11 µm sliding against each other are of the order of a few micronewtons. The microbalance was equipped with an inner chamber to protect test samples from contaminants and to perform experiments in specific environmental conditions (humidity of 45%, and 25°C). The data acquisition and control station allowed force measurements at the sample weighing position, as a function of the vertical displacement of the platform.

During friction force measurements the vertical fiber was connected to the microbalance at the sample weighing position (see Fig. 3 A) and a load of 1 mg was applied at the other end of this fiber so as to maintain it in a vertical position. The horizontal fiber was fixed to a metallic holder, and brought into contact with the vertical fiber until the deflection angle of the vertical fiber was equal to 2.3°, which is also equal to the wrap angle of the horizontal fiber by the vertical one. The platform was then raised at a fixed speed of 2 µm/sec which induced sliding of one glass fiber against the other one. The force was recorded by the balance as a function of the vertical displacement of the platform. The total sliding distance along the vertical fiber was fixed to 2 mm.

2.2.1 Typical curve obtained

The experimental curve stick-slip curve obtained is quite irregular (see Fig. 3B). A detailed statistical analysis of the force curves was carried out using a computer program.

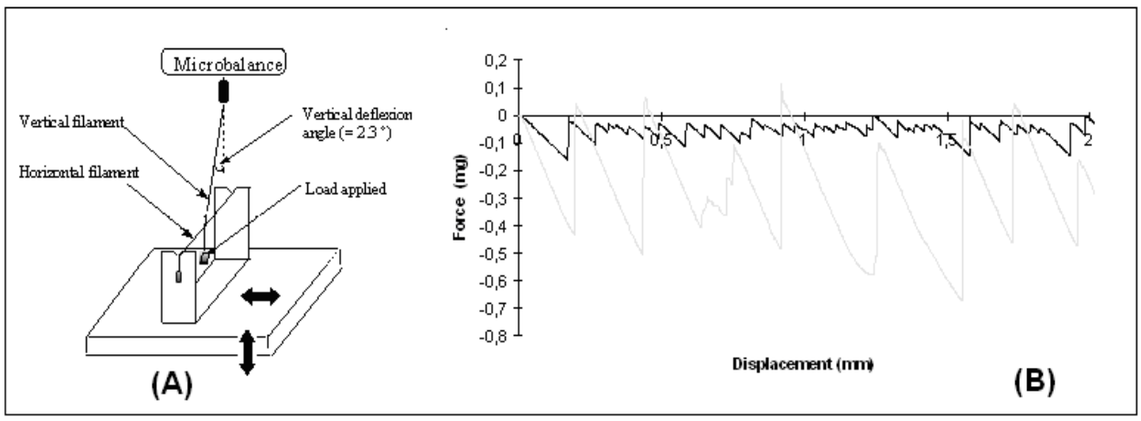

Fig. 3. (A) : Experimental set-up for friction measurement of two crossed glass fibers : the deflection angle of the vertical fiber connected to the microbalance is 2.3°, the horizontal fiber is fixed to a fiber-holder B) Stick-slip friction curve profile of fiber A (in dark line) and of fiber E (in grey line); the change in force is plotted against the vertical displacement of the horizontal fiber.

Static friction force values were obtained from the minimum values of the curve because, at the start, the microbalance platform was constrained to move upwards, and consequently static friction force values measured had negative values. So the signs of the friction force values were inverted. Moreover, before the vertical displacement of the platform, the balance was set to zero, while in practice, there was a load N at the extreme end of the vertical fiber. The real static (or dynamic) friction force measured was then (-Fs+ N).

2.2.2 Static friction coefficients

Capstan method generally applied for yarn-yarn friction measured by the F-meter was used to calculate the static friction coefficients during fiber-fiber motion (Gupta, 1993):

$$\mu = \frac{Ln\frac{T_2}{T_1}}{\alpha} \tag{3}$$

'T_1' is the initial tension, that is the load applied to the vertical fiber + the fiber weight

'T_2' is the real static force measured. (-F_s+ N). The wrap angle 'α' is equal to the deflection angle 'θ' of the vertical fiber for small values of deflection angle (see Fig. 3A). The deflection angle of the vertical fiber was calculated for each vertical displacement 'Z' of the horizontal fiber before calculating the friction coefficient

3. Results and discussions

3.1 Results of LFM analysis of fibers

Images obtained in the AFM mode (topography) and in the LFM mode are presented in figures 4, 6, 7 & 8. The difference between the LFM backward and forward signals gives twice the friction force in volts. Friction coefficients were calculated by dividing the friction force (in nN) by the normal applied force (in nN), the latter being calculated and calibrated by using the contact force curve profile (see Fig. 5A), as described earlier. For each fiber, numerous tests were performed and the friction coefficient values were found to be reproducible when tests were carried out on different regions of a filament as well as on different filaments of the same glass fiber.

The friction coefficient values were found to be relatively small and varied from 0.01 to 2. These are relevant values, especially when we compare them to those obtained by other authors (Bhushan, 1985) who worked on polymeric films and other surfaces. As compared to film-film friction coefficient values for PET for example which are around 0.66-0.77, nanoscale friction coefficients of PET films measured by AFM/LFM are relatively small and are around 0.02-0.06.

3.1.1 Desized glass fiber

Glass fiber without size was equally analyzed by AFM/LFM. A desizing procedure was established, which consisted in heating the sized fiber at 600°C for 24 h so as to completely destroy the organic size. The topographical image (Fig. 4) shows that the desized fiber surface has a friction coefficient μ= 0.04 which stays constant all throughout the fiber

surface. Fig. 5C shows that there is a great attraction of the tip by the sample before the former may be in contact with the fiber. This phenomenon may be explained by a higher surface energy of the clean desized glass fiber which is going to attract water molecules of the air very rapidly. Indeed, molecules of water form a film of water at the fiber surface, and this acts as a lubricant—hence, the very weak value of the friction coefficient.

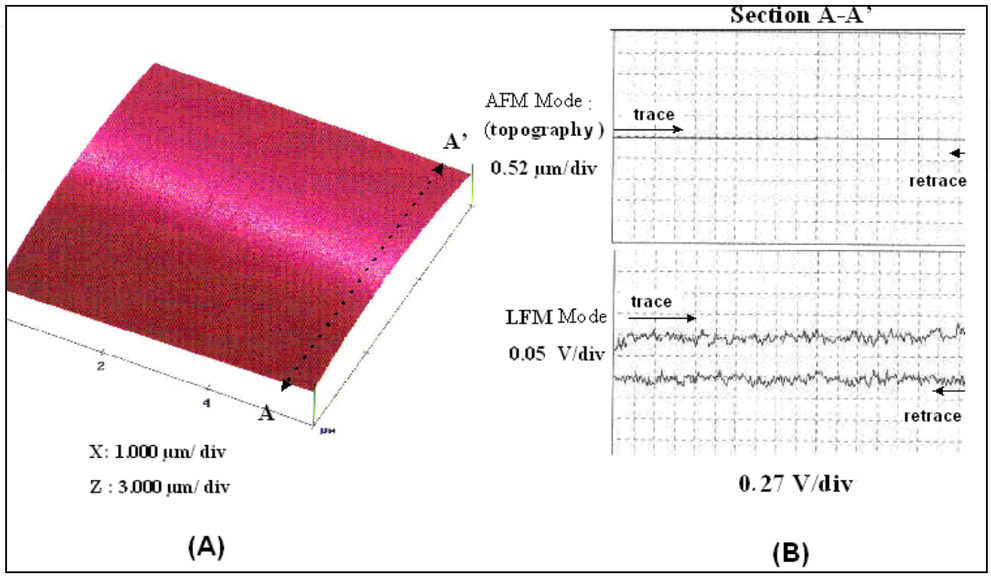

Fig. 4. Desized glass fiber: (A) topographic image; (B) scope-mode forward and backward scanned AFM and LFM signals of section A–A'.

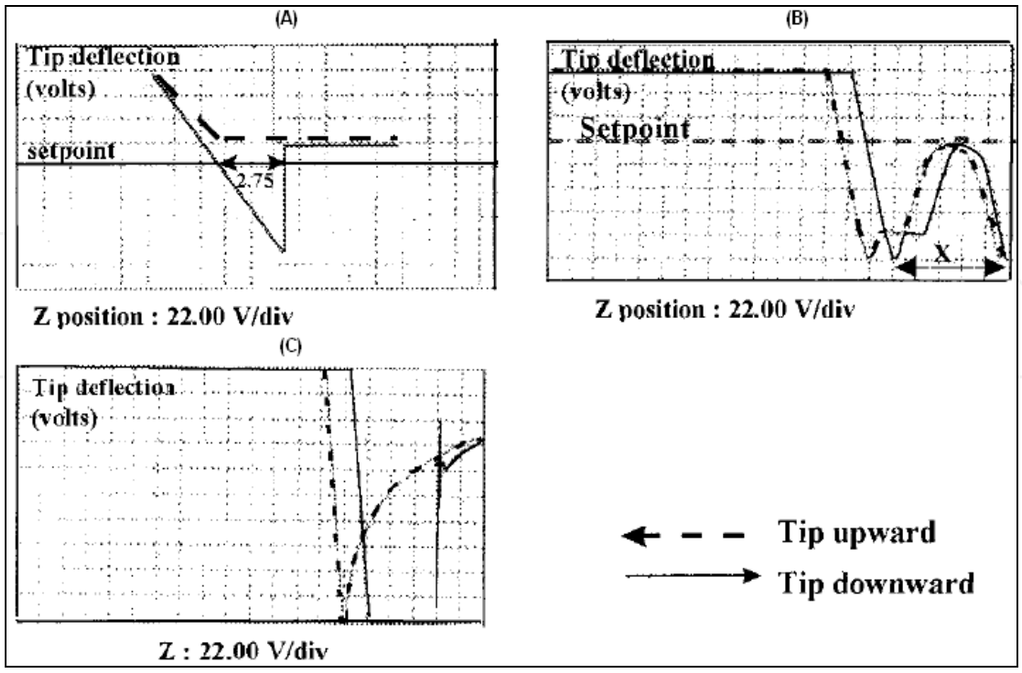

Fig. 5. (A) A normal contact force profile, (B) Contact force profile during scanning of fiber E and of (C) the desized glass fiber

3.1.2 Sized glass fibers

All sized glass fibers have very heterogeneous surfaces compared to the plain surface of the cleaned glass fiber.

3.1.2.a Fiber A

Typical images of fiber A, obtained in the AFM and LFM modes are illustrated in Fig. 6A and 6B, respectively. These have been obtained at a contact force of 38 nN. The topographic image in Fig. 6A, shows randomly distributed bumps of variable dimensions. The forward and backward scanned images in the LFM mode presented in Fig. 6 B, show that contrasts on the bumps are reversed when the scanning direction is changed. The scope mode AFM and LFM signals of the sections A-A′ and B-B′ corresponding to extremities of the topographic image of Fig. 6A are illustrated in Fig. 6C and 6D respectively. The scope mode LFM signals of the bumps reveal a friction force (F_f) of ~0.035 Volts (indicated by full lines), that is a friction coefficient μ ~0.04. The remaining surface (indicated by dashed lines) has a friction force two to three times greater, that is a friction coefficient μ~0.12.

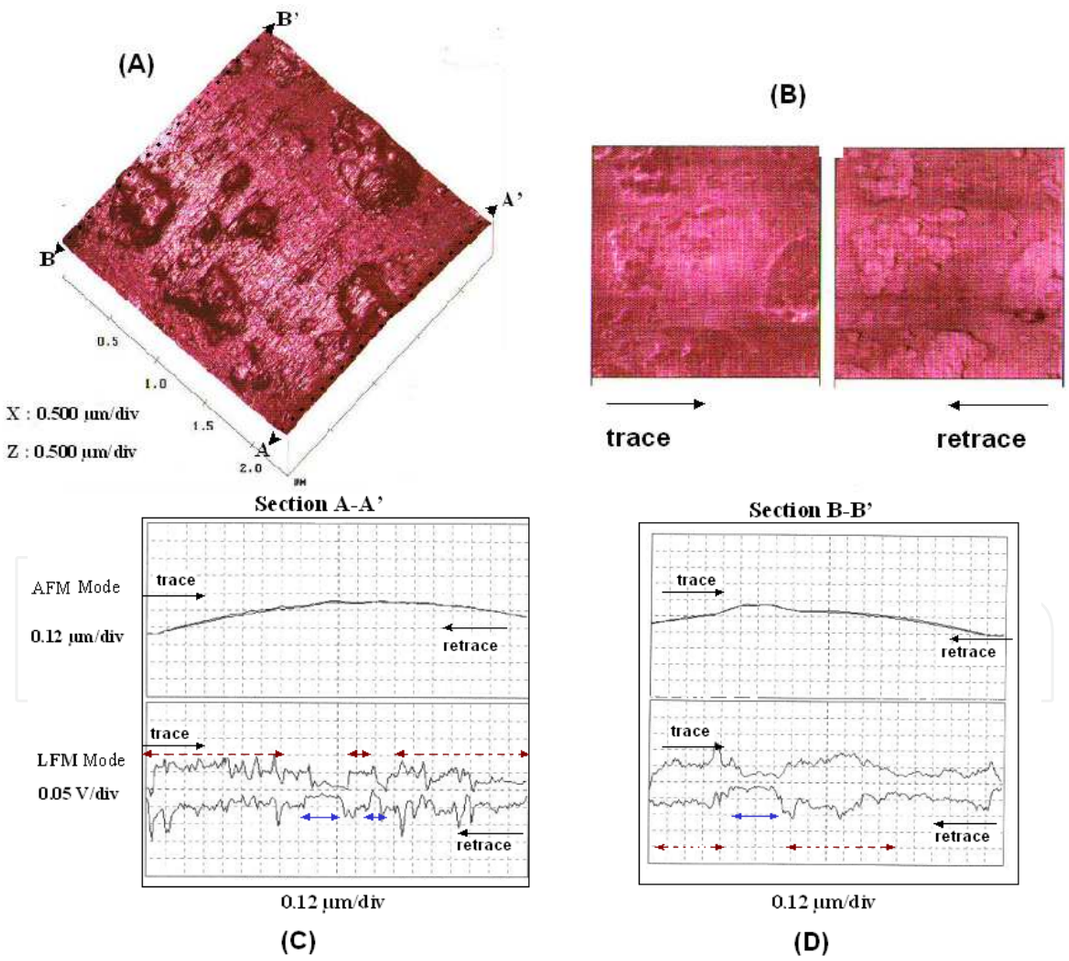

Fig. 6. Fiber A: (A) topographic image; (B) forward and backward scanned LFM images; (C) scope-mode forward and backward scanned AFM and LFM signals of section A–A′ and of section B–B′ (D)

Furthermore, in the LFM mode, small fluctuations of the backward and forward signals were observed. Friction forces were determined by considering the average value of signals, only.

The glass fiber with the size A presents therefore, a physically and chemically heterogeneous surface, with bumps having a friction coefficient μ~0.04 while the overall surface has a friction coefficient μ~0.12. This would mean that during coating of glass fiber A by the starch size, the different constituents of the size are not distributed in a homogeneous manner.

3.1.2.b Fiber E

When the topographic images were realized at a contact force greater than 70 nN, surface damage due to plowing of the size E by the AFM tip, was observed. A typical example of such topographic images is illustrated in Fig. 7A.

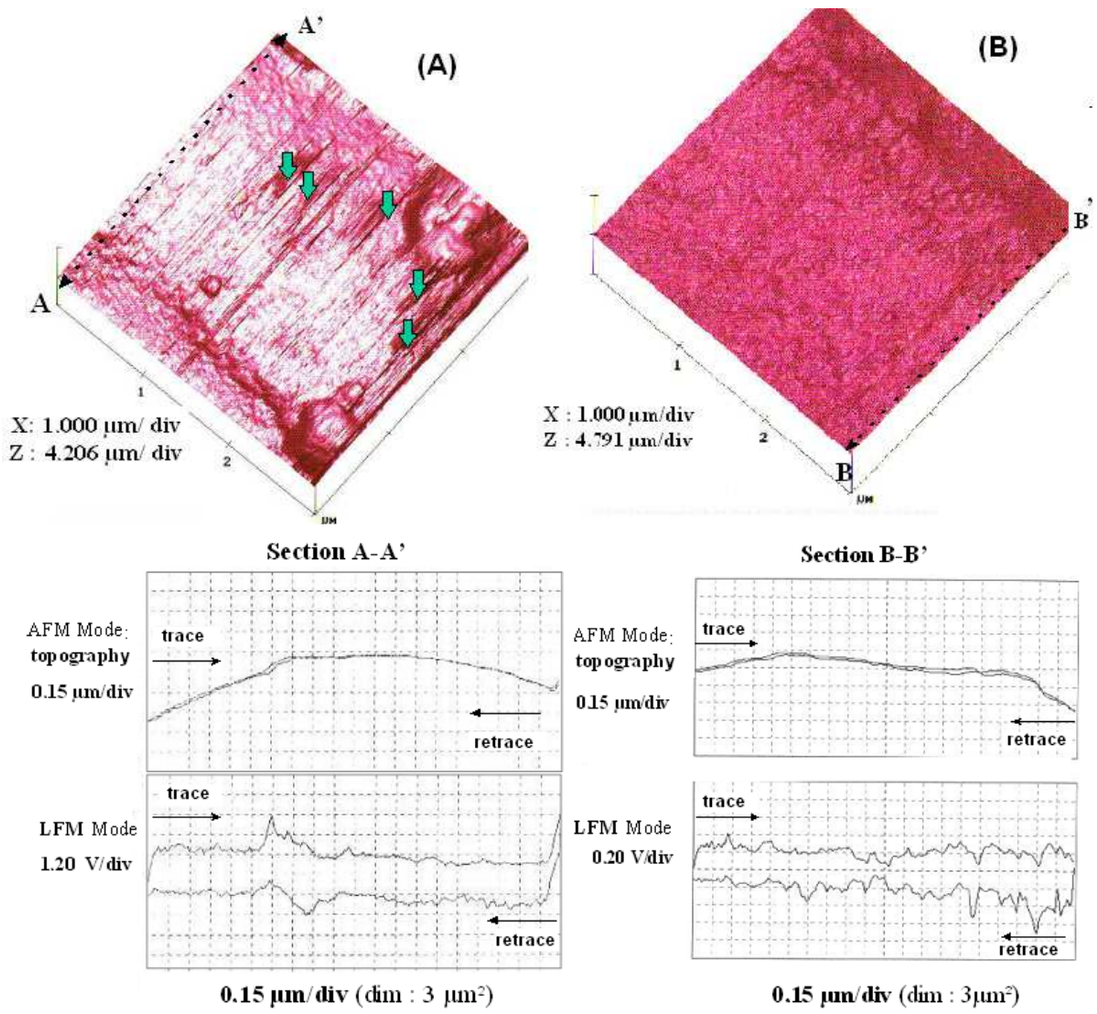

Fig. 7. Topographic image of fiber E, E4 and scope-mode forward and backward scanned AFM and LFM signals of section A–A'for fiber E, and of section B–B'for fiber E4. (plowing positions of fiber E are indicated by arrows)

Moreover, the contact force profile which gives the deflection signal as a function of the distance between the AFM tip and the fiber sample (as the piezodrive moves upwards and then downwards), shows that the AFM tip remained stuck to the size, and it was difficult to pull-off the tip from the fiber surface (Fig. 5B).

An example of topographic image of another fiber taken from the same roving of fiber E4, where plowing did not occur, is shown in Fig. 7B. The latter was made at a contact force of 62 nN and the contact force curve profile was normal. The difference between the forward and backward LFM signals revealed a constant friction coefficient of 0.2 throughout the fiber surface. This value is greater than that of the starch size on fiber A, for which the maximum friction coefficient is around 0.12.

The fact that some fibers are readily plowed by the AFM tip while others are not, may indicate a difference in the degree of cross-linking of the epoxy film-former of the size on fiber E, among fibers of a same roving.

When fiber E was annealed at 100°C for 60 h, the topographic image realized at 46 nN (Fig. 8A) shows no presence of plowing, and the contact force calibration curve profile was normal (see Fig. 5A). Nevertheless, it reveals an aggregation of matter with the formation of small blisters (indicated by arrows) of diameters of approximately 0.15 µm. LFM signals of a 1-µm² scanned area (Fig.8B) of a blister (full line) reveal a friction coefficient of µ= 0.03 which is smaller than that of the general surface of µ= 0.09.

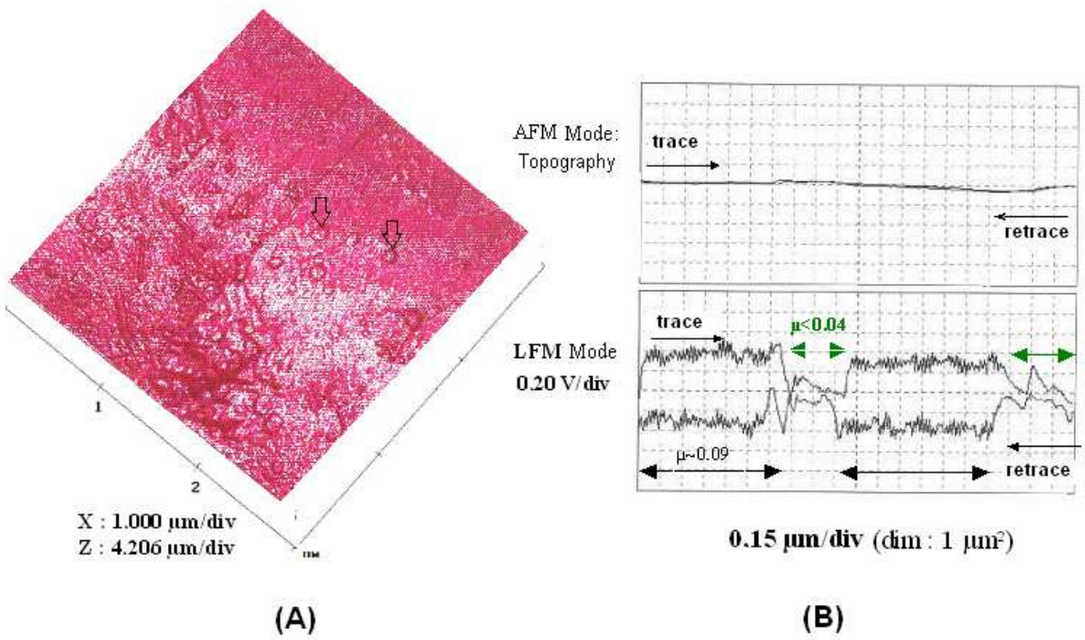

Fig. 8. Annealed fiber E41: (A) topographic image; (B) scope-mode forward and backward scanned AFM and LFM signals.

According to the observations made on the annealed glass fiber E4, in both the AFM and LFM modes, it can be said that the increased crosslinking of the epoxy resin by annealing leads to a sized surface having a higher surface Young's modulus. The size is therefore less susceptible to be plowed by the AFM tip. One can also emit the hypothesis that during an

increased crosslinking of the epoxy film former the lubricant is expurgated off onto the external surface in the form of blisters. This would have, consequently, the effect of decreasing the coefficient of friction (μ = 0.03).

3.2 Fiber-fiber friction force measurements by the electronic microbalance

Results for measurements carried out under the following fixed conditions of constant speed (2 μm/sec), load (1 mg), relative humidity (45%), and temperature (25°C), are presented. Fig. 3B shows typical stick-slip curves for two different fibers A and E, obtained by plotting force as a function of the vertical displacement of the horizontal fiber. The stick-slip events for fiber E, are characterized by a greater average amplitude and a smaller frequency than those of fiber A. However, when each friction curve is considered in more detail, stick-slip irregularities along a filament as well as from one filament to another are observed. To obtain a 95% confidence level, friction measurements were carried out on four different segments of 3 mm long filaments from five randomly chosen filaments.

Static friction coefficient (μ_s)

Fig. 9 shows the histograms of frequency distribution of static friction coefficients "μ_s" of fibers A and E respectively. For fiber E, the "μ_s" values follow a normal distribution with a mean value around 5 and a standard deviation of 1.7. However, for fiber A, a bimodal distribution of "μ_s" values is observed, with a mean value of the first distribution situated around 2 and that of the second distribution around 6.

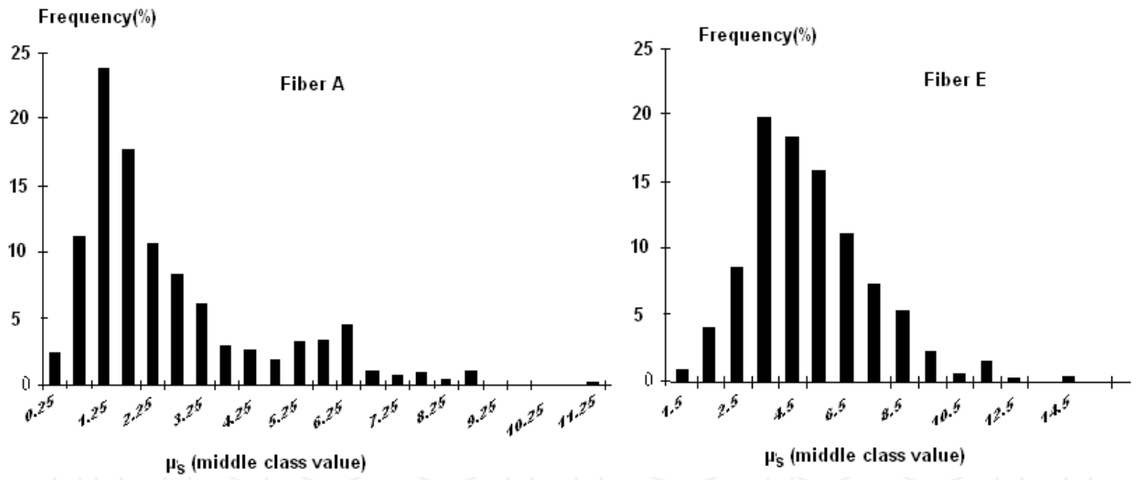

Fig. 9. Histogram of static friction coefficients of fibers A and E, measured by electronic microbalance

3.3 Comparison of fiber-fiber friction to friction analysis of surfaces by LFM

The greater static friction coefficient values of fiber E (than the fiber A), during fiber-fiber friction can be explained by the greater frictional values detected by the LFM technique. However, as the LFM signals reveal no chemical heterogeneity of the fiber E surface (constant friction coefficient of 0.2), the great standard deviation of friction values during fiber-fiber friction can be attributed to the surface roughness of fiber E: this leads to different contact area each time a fiber is in contact with an another one.

In the case of fiber A, in addition to surface roughness, chemical heterogeneity due to two regions with different friction coefficients (0.04 and 0.12) was observed by LFM. The great standard deviation of "μ_s" as well as its bimodal distribution, during fiber-fiber friction are thus due to surface roughness and chemical heterogeneity.

The low friction coefficient values obtained by LFM may be explained by the fact that sliding of AFM tip on a fiber sample surface is easier ($\mu < 1$), than that of a fiber on another fiber surface (μ_s~1-10). Moreover in LFM, the friction force analyzed is a dynamic one, while in this case, it is the static friction coefficient which is being evaluated. The friction coefficient values disparities can be related to scale difference of measurements and to the nature and surface of contact which are different in both cases. In AFM, a Si_3N_4 tip having a radius of curvature of about 30 nm, is in contact with the fiber surface while during fiber-fiber friction measurements sized fibers of diameter 11 μm are in contact.

3.4 Determining the theoretical contact area during the fiber-fiber friction

The theoretical contact area during friction, can be calculated by using the DMT and JKR theories of contact mechanics. But according to Pashley, as the glass fiber is rigid and the fiber radius as well as its surface energy small, the DMT theory should be applied (Pashley, 1984). For orthogonally placed fibers, if contact occurs at one point, the contact radius derived by the DMT is 0.118 μm . However, contact between the two fibers occurs on a length of a circular arc of $2\pi r\ (\theta/360)$ (where the wrap angle θ=2.3° and the fiber radius: r=5.5 . 10^{-6} m (see Fig. 3). Thus the area of contact 'A' between the two fibers is approximately an ellipse, and it is evaluated to be A=0,12 μm² (details of this result is published in another paper (N. Behary et al., 2000).

3.5 Types of contact possible during the fiber-fiber friction of the fiber A

The AFM/LFM measurements of the fiber A revealed two regions of distinct friction coefficient (μ~0.04 and 0.12 respectively), each of them having a surface area comprised between approximately 0.1 and 1μm², that is nearly the same contact area as that during fiber-fiber friction. Thus, the main types of contacts that can take place would have the configurations illustrated in Fig. 10.

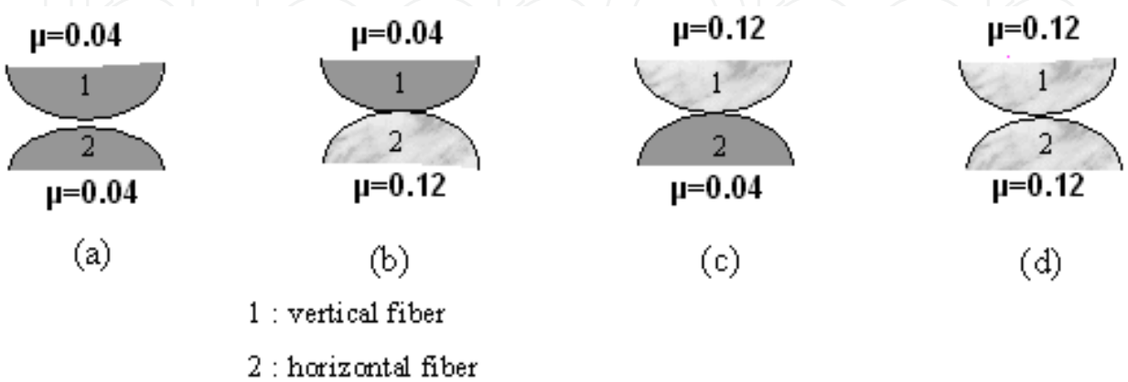

Fig. 10. Modelling the different contacts possible during fiber-fiber friction of the sized fiber A (the friction coefficients are those evaluated by LFM)

Globally therefore, there can be four different types of contact during the fiber-fiber friction. We can compare these configurations to the results obtained by Yamaguchi (Yamaguchi, 1990) for polymer-polymer and polymer-steel friction force measurements. Yamaguchi observed that the friction coefficient of any polymer against PTFE (polytetrafluoroethylene) was nearly the same and of a small value (μ~0.1), while the friction of a polymer against steel varied a lot. In fact, it is the polymer presenting a weak friction coefficient that imposes the value of the relative friction coefficient (in the limit of the study considered). Therefore it can be concluded from our study that contacts a, b and c lead to a relative weaker friction coefficient than contacts of the type d. This would lead to a bimodal distribution of the relative friction coefficients during fiber-fiber friction and would explain our experimental results.

4. Conclusions

In light of the above results and discussions, both techniques of measuring friction forces, by Lateral force microscopy and an electronic microbalance, seem to be invaluable methods for characterizing frictional properties of sized glass fibers. The AFM/LFM successfully determines the topography and chemical nature of sized and desized glass fibers. Sized fibers have both physical and/or chemical heterogeneities while the desized bare glass fiber is completely plain and smooth.

AFM/LFM results also help to better understand friction force results obtained at a larger macro scale, particularly the widespread values of friction coefficients during fiber sliding. Nanosccale friction values by AFM/LFM are smaller than 'micro' friction values during fiber-fiber friction because the nature and the area of contact are different in both cases.

Part II: Air-atmospheric plasma treatment of PET (Polyethylene Terephtalate) woven fabrics studied by atomic force microscopy

1. Introduction

Polyester fabrics made from PET poly(ethylene terephtalate) account for almost 50% of all fiber materials. PET fibers have high uniformity, mechanical strength or resistance against chemicals or abrasion. However, high hydrophobicity, the build-up of static charge, stain retention during laundering and being difficult to finish are undesirable properties of PET.

Enhancement of the hydrophilicity of PET fibers is a key requirement for many applications, ranging from textile production to applications in the biomedical field. In the textile field, increased hydrophilic properties improves comfort in wear with a better moisture management due to increased wettabilility, wicking, adhesion to other materials (i.e. coating), and dyeing (Pastore M, 2001). Several strategies can be adopted to increase the surface energy and hence the hydrophilicity of PET fibers such as by chemical finishing or grafting, chemical surface treatment with NaOH (Collins, 1991, Haghighatkish, 1992), biochemical treatment with enzymes (Vertommen, 2005) or physical surface treatment using plasma. Treatment with NaOH is environmentally unfriendly and causes drastic weight and strength losses (Collins, 1991), while certain plasma treatments would be of interest from an environmental point of view.

Plasma techniques have been used in materials science since 1960s, for the activation and modification of different materials. Plasma processes have been utilized to improve the surface properties of fibers for various textile applications: sterilization, desizing, wettability or hydrophobicity improvement, anti-shrinking finishing, dyeability enhancement and adhesion promotion (Hocker 2002, Jasso, 2006, Leroux, 2006, Oktem, 2000). The fibers that can be modified by plasma processing include almost all kinds of fibers such as natural and man-made, metallic fibers, glass fibers, carbon fibers and organic fibers (Höcker, 2002, Borcia, 2003). Low-pressure plasma methods have been investigated, but they are difficult to apply in industry since they require vacuum and consume a considerable amount of energy. Moreover, these treatments can be carried out only in a batch process which increases the treatment time. New methods based on atmospheric plasma treatments seem to be quite attractive for the textile industry. These treatments have the advantage of being applied on-line without vacuum, and allow continuous plasma processing (Leroux, 2006). Atmospheric plasma treatments are used to modify polymer surfaces using plasma gases made up of a mixture of charged particles (electrons and ions), excited atoms (free radicals, meta-stable molecules) and photons. In order to create a plasma field, the gases are brought through two charged electrodes of different potentials. During plasma treatment, the polymer to be treated is exposed to the plasma which interacts and modifies the polymer surface. Surface modifications vary with the nature of the substrate and the chemistry of plasma gases, as well as the treatment operating parameters (Borcia, 2004, Leroux, 2006,)].

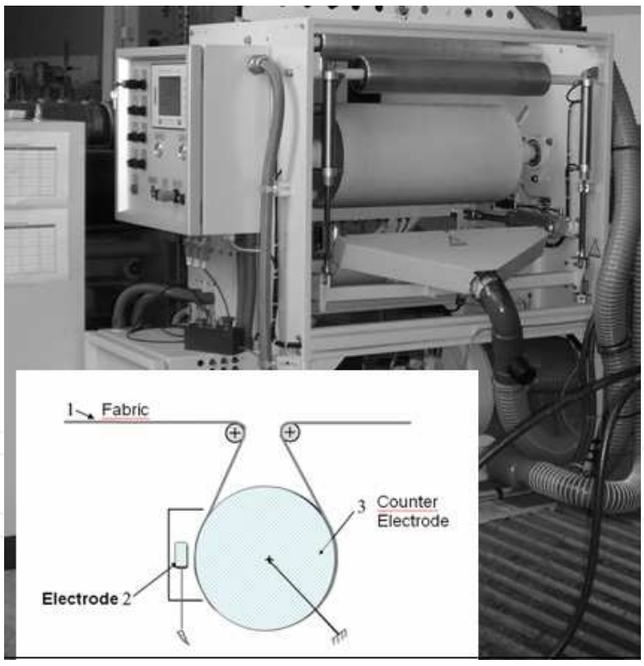

Fig. 11. Plasma treatment under atmospheric pressure by means of dielectric barrier discharge, using "Coating Star" plasma machine manufactured by the Ahlbrandt System Company

Among various atmospheric pressure non-thermal plasmas, the dielectric barrier discharge (DBD) process is studied mostly for the easy formation of stable plasmas and its scalability. Numerous studies of surface modified materials using DBDs under atmospheric pressure have been undertaken mainly for treatment of polymers and metals. The dielectric barrier

discharge (DBD) is created between two metal electrodes covered with insulating layers (ceramic and polycarbonate). Under specific conditions, the DBD can produce the so-called atmospheric pressure glow (APG) discharge, which can also be effectively used for the surface treatment (Borcia, 2003, Fang, 2004).

Studies show that the highly reactive species in the discharge regime of DBDs can interact with the surfaces of materials and induce some physical and chemical changes (oxidation, polymerization, cross-linking, etching etc) and thus improve their surface properties such as wettability, printability, adhesion and conductivity (Oktem, 2000, Fang, 2004).

Ageing of surface-modified polymers can be detrimental to the performance of a device. Therefore an improved understanding of the ageing of modified surfaces during storage is required to optimize the processing conditions leading to interfacial properties that are controlled and predictable at the time of use. It has been shown that as a result of ageing, the surface properties, acquired after a plasma treatment, disappear (Krump, 2005). Moreover, ageing survey data (Borcia, 2004) show that materials never fully return to their untreated surface state. The ageing effects observed depend on the nature of the polymeric materials, structure, crystallinity, (Novak, 2004) porosity etc. Additionally, it has been reported (Leroux, 2006), that the fabric porosity which depends on the fabric structure (e.g. woven, nonwoven, knitted) influences the ageing of air-atmospheric plasma treated fabrics subjected to aqueous conditions at room temperature and pressure. It was also shown that for a low porosity-(high density) woven fabrics, oxidised species formed at the fabric surface are more easily removed by simple washing than for high porosity textile structure.

The work presented here demonstrates the potential use of Atomic Force Microscopy to optimize the atmospheric plasma process parameters (speed treatment and electrical power) on the treatment of a particular woven PET fabric. The effect of ageing during normal use conditions (i.e room temperature and pressure in absence and presence of day light) and in conditions used for dyeing polyester fabrics, has equally been studied. PET fabrics are dyed with disperse dye and need high temperature (130°C) and pressure for maximum dye uptake. Dyeing at 90°C would be more environmentally friendly because of reduced energy requirements, but dye uptake would be reduced. One of the strategies to increase dye uptake at 90°C is to activate the PET fabric surface by plasma treatment so as to increase its hydrophilicity. It is therefore necessary to check the permanence of the air-atmospheric plasma treatment of PET fabrics for specific dyeing conditions.

In the final part, the effect of immobilizing a hydrophilic oligomer PEG -poly(ethylene glycol) 1500 immediately after plasma treatment is shown. AFM results are also compared to other fabric surface characterization methods such as water contact angle, capillary uptake, and XPS (X-Ray Photoemission Spectroscopy).

2. Experimental work

2.1 Sample preparation

2.1.1 Woven polyester fabric

A 100 % Polyester (PET) woven fabric of density 284 g/m² with a thickness of 0.56 mm and 63.5% porosity was used for the study. The PET woven fabric was cleaned to be free from surface impurities and spinning oil. The cleanliness of the PET samples was checked by

measuring the surface tension of final rinsing water (used to clean the PET samples), which remained constant and equal to 72.6 mN/m ,which is the surface tension of pure water.

2.1.2 Sample preparation for plasma treatment

The PET woven fabric was cut into square pieces of 50cm X 50cm on the basis of the electrode length of the plasma machine (50 cm). The speed of the fabric in the discharge zone could be varied through the control.

2.1.3 Plasma treatment of woven PET samples

All plasma treatments were carried out using an atmospheric plasma machine (see Fig. 12) called 'Coating Star' manufactured by Ahlbrandt System (Germany). The following machine parameters were kept constant: electrical power of 1 kW, frequency of 26 kHz, electrode length of 0.5 m and inter-electrode distance of 1.5 mm. The outer layer surfaces of both electrodes were of ceramic (a dielectric material), so that when these electrodes were subjected to a potential difference, a glow discharge called the 'Dielectric Barrier Discharge' (DBD) was created.

(a)

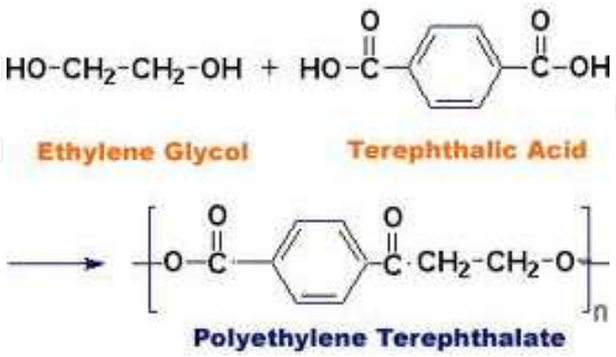

(b)

Fig. 12. (a) Optical microscopic view of the PET woven fabric, (b) chemical formula of PET

Atmospheric air was used during the atmospheric plasma treatments. The textile samples were subjected to varying plasma Treatment Power (TP) which is the plasma power applied

per m² of textile sample, expressed in kJ/m². The TP is related to the velocity of the treatment (V) and the electrical power (P) of the machine, by the equation (Eq. 1):

$$TP = \left(\frac{P}{V \times L} \right) \times 0.06 \quad (1)$$

P = Electrical Power (W)
L = Electrode length (m)
V =Velocity of the sample (m/min)

Plasma treatment was carried out at velocities (V) of 1 m/min, 2 m/min, 5 m/min and 10m/min. It was also performed at constant speed with varied electrical power (P) of 400 watts, 700 watts and 1000 watts. After plasma treatment, each plasma treated sample was separated from waste fabric and kept in aluminium foil away from light.

2.1.4 Ageing methods

Effect of ageing on air-plasma treated PET fabric samples was observed by monitoring changes in water contact angle as well as surface topography of the samples, 20 days after plasma treatment. Ageing of plasma treated sample was carried out in two different ways:

- *Without light:* Plasma-treated samples were kept folded in aluminium foil and stored in cupboard, in a small dark chamber to avoid contact with light.
- *With light:* Plasma treated samples were kept open in laboratory conditions allowing them to be in contact with light. Laboratory conditions with a temperature of 20 ± 2°C and relative humidity of 60± 10 % were maintained during the experiment.

2.1.5 Effect of PET fabric dyeing conditions (High temperature conditions)

The plasma treated PET samples were immersed in aqueous conditions at 90°C for 30 minutes without the presence of any dye.

2.1.6 Effect of adhesion of PEG 1500 on PET fabric

As ageing with time causes loss of hydrophilic species formed by plasma treatment (Krump, 2005), immobilizing a hydrophilic oligomer like PEG -poly(ethylene glycol) immediately after plasma treatment would perhaps yield a more durable hydrophilic treatment. PEG-poly(ethylene glycol) has been used for surface modification because of its unique properties such as hydrophilicity and flexibility (Harris, 1992).

PEG of molecular weight 1500 g/mol , i.e PEG 1500 from Fluka chemicals was immobilized on cleaned-untreated PET fabrics as well as plasma treated PET fabric samples using padding and curing method. For the padding process the open-width PET fabric was passed through an aqueous solution of PEG 1500 in water and through two squeezing rollers (see Fig. 13). At a squeezing pressure of 4 bars, the weight pick up remained almost constant around 56%.

2.2 AFM tapping mode images

In a previous paper Leroux and al. (Leroux, 2006) showed using AFM in the LFM mode, that friction forces measured at the surface of PET fabric is doubled after a plasma

treatment, and these forces remain homogeneous throughout the plasma treated PET fiber surface.

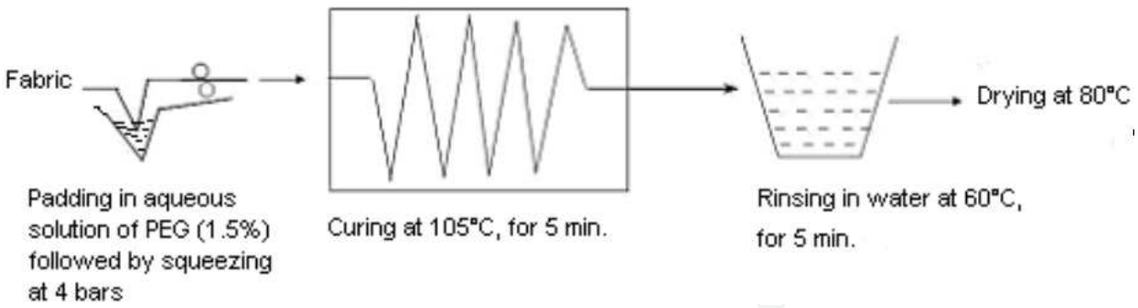

Fig. 13. Application procedure of PEG-1500 on PET fabric by padding, squeezing followed by curing and a final rinsing before drying.

In this chapter, surface investigation by imaging in the Tapping mode using AFM "Nanoscope III" from Digital Instrument, is presented. This mode was preferred to the AFM /LFM (contact mode AFM), since the Tapping mode overcomes problems associated with friction, adhesion, electrostatic forces which may arise after a plasma treatment, and which would distort image data (Kailash, 2008).

Tapping mode imaging was carried in ambient air using 'Budget sensor' tips from 'Nanoandmore', of length 125 μm, made of $Si_3 N_4$ with aluminium coating, and a resonance frequency of 300 kHz. The cantilever which scans the surface is oscillated at or near its resonant frequency using a piezoelectric crystal. The oscillating tip is moved toward the surface until it begins to lightly touch, or tap the surface, significantly reducing the contact time. During scanning, the vertically oscillating tip alternately contacts the surface and lifts off, generally at a frequency of 5000 to 500,000 cycles per second. As the oscillating cantilever begins to intermittently contact the surface, the cantilever oscillation is necessarily reduced due to energy loss caused by the tip contacting the surface. The reduction in oscillation amplitude is used to identify and measure surface features. When the tip passes over a bump in the surface, the cantilever has less room to oscillate and the amplitude of oscillation decreases. Conversely, when the tip passes over a depression, the cantilever has more room to oscillate and the amplitude increases (approaching the maximum free air amplitude). This feed back signal also allows construction of the topographic image. The fiber surface roughness Ra was calculated directly from AFM signals (Feninat, 2001) using the software supplied with the Nanoscope III.

2.3 Water contact angle and capillary measurements

The sessile drop method is useful for measuring water contact angles greater than 90° however for lower contact angles the porous woven fabric immediately absorbs the liquid drop. That is why wettability of textile surfaces was monitored indirectly through a wicking test using a tensiometer. This method allows the measurement of contact angle as well capillarity measurements. The tensiometer used is the 3S from GBX, France. During measurements, a vertically hanging fabric sample of defined dimension is connected to the tensiometer at the weighing position and progressively brought into contact with the

surface of water placed in a container. On immediate contact with the water surface, a sudden increase in weight (W_m) is measured due to meniscus formation on the fabric surface. The weight increases further as the liquid flows inside the fabric structure by capillarity (wicking). The capillary weight (W_c) after 6 minutes, is measured. From the meniscus weight (W_m) the water contact angle can be calculated. More detailed description of this experiment can be found in our previous work (Leroux, 2006).

3. Results and discussions

3.1 Effect of varying speed and electrical power on plasma-treatment of PET woven fabrics

Irrespective of treatment power and speed setting, the water contact angle after plasma treatment was always around 45°, while the untreated PET fabric water contact angle was 80°. Any decrease in speed or increase in Treatment Power did not have a significant impact on this minimum contact angle value. However, tapping mode AFM images of samples (Fig. 14) subjected to an air–plasma treatment at varying Treatment powers "TP" of 0, 12, 24, 60 and 120 kJ/m² show considerable changes in fiber surface morphology.

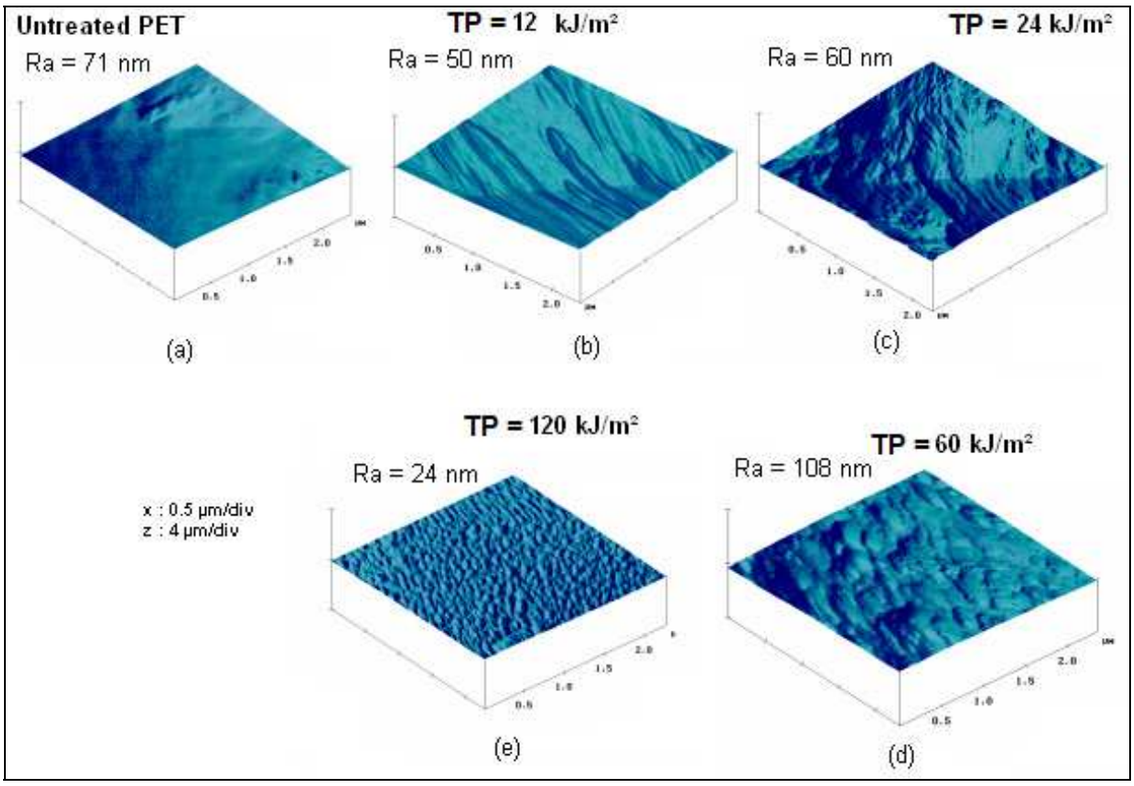

Fig. 14. Topographic images obtained by AFM in the tapping mode of a) an untreated PET fabric fiber surface, a plasma-treated PET fabric fiber surface at treatment power ''TP'' of (b) 12 kJ/m², (c) 24 kJ/m² , (d) 60 kJ/m² and (e) 120 kJ/m² (Takke, 2009).

Fig. 14 shows that as the treatment power is increased from 0 to 120 kJ/m² there is significant surface restructuring. At very low Treatment Power of 12 kJ/m² at a speed of 10

m/min, a smoother surface is obtained observable as a decrease in surface roughness, Ra=50 nm, (Fig. 14 b). The smoother surface at this highest speed and low plasma power, may be due to etching of the very upper layer of the PET surface. However, as the Treatment Power is further increased to 24 KJ/m² at a lower speed of 5 m/min, further etching of the PET surface creates disordered bumps (Fig. 14c). Continued increase of TP to 60 KJ/m² at a lower speed of 2 m/min, leads to more uniform scale-like structures (6 scales per µm, Fig. 14d) which increases the surface roughness of the fiber, Ra= 108 nm. Further increase in TP to 120 KJ/m² (at 1 m/min) causes further uniform etching yielding tinier, more organized, uniform and flatter beads (12 beads/µm, Fig. 14e) leading to a decrease in the surface roughness (Ra=24 nm).

The increase in hydrophilicity of the PET fabric surface after the atmospheric-air plasma treatment is probably due to plasma oxidation, which destroys the surface chemical bonds, leading to an increase in polar groups (Borcia, 2003). Plasma treatments generate polymer chain-scissions of the weakest bonds of the polyester, creating very reactive chain-end free radicals. These radicals then react easily with the reactive species (ex: oxygen radicals) present in the plasma generating polar species such as carbonyl, carboxyl and hydroxyl groups, which are polar species capable of increasing the surface energy (Leroux, 2006). We have previously reported using X.P.S measurements (X-Ray Photoemission Spectroscopy) (Leroux, 2009) that there is an increase in concentration of oxygen at the fabric surface after air plasma treatment of the PET fabric, and this would explain the increase in surface energy of the fabric surface.

The plasma treatment not only causes chemical modifications of the PET surface by adding polar groups, but also morphological surface changes that are observed by tapping mode AFM imaging. Although the lower water contact angle (45°) is measured even at low Treatment Power (12 kJ/m²), surface etching of the PET fiber surface continues with increasing Treatment Power, yielding an increased surface roughness. At higher Treatment Powers (60 and 120 kJ/m²) a more organized scale–like surface structure is observed

3.2 Effect of ageing on plasma treated PET sample

Ageing of atmospheric plasma treated PET woven fabric with TP of 60 KJ/m² in the absence and presence of light was evaluated. In absence of light, very little change in water contact angle was observed. However, there were substantial increase in water contact angle (45° to 73°) and decrease in capillary weight for plasma treated PET fabrics kept in presence of daylight. The increase in contact angle with time, in presence of light, could be due to the loss of surface oxidation species at the plasma treated PET fabric surface. Degradation of peroxide radicals due to UV rays of the daylight could be a major factor in increasing the water contact angle of the plasma treated fabric (Takke, 2009).

Tapping mode AFM imaging carried out after the 20th day of ageing in the absence of light shows that there is deformation of the scale-like structures formed as a result of plasma treatment at 60 KJ/m² observed as a disordered surface structure with big bumps. In presence of light, smaller, flatter and fewer blister-shaped structures, of different sizes, appear as if, the scales formed by plasma treatment had been nearly completely eroded, leaving a smoother (Ra =52 nm).

While in absence of light slow ageing initiates a disordering of the surface, ageing in presence of light leads to an organized structure. Without light, the ageing process proceeds slowly as evidenced by the similar water contact angles of the 20 and 1 day samples. As only slight change in the surface topography is observed, the oxidised species should stay on the fiber surface and are not removed by ageing without light. With light, the ageing process seems to be accelerated, both at the outer fabric surface and the inner fabric fiber surface.

Further chemical analysis of the surfaces for example by XPS (X-Ray Photoemission Spectroscopy) would provide clearer information on the effect of light on plasma treated samples, however AFM imaging seem to be an invaluable tool to investigate ageing effect on surface structuring.

3.3 Effect of PET fabric dyeing conditions (High temperature conditions)

Plasma treatment alone increases the hydrophilicity of PET fabric, demonstrated by the decrease in water contact angle from 80° to 45°. However, after 30 minutes of immersion in water at R.T.P there is an increase in water contact angle from 42° to 55°, and a considerable decrease in capillary weight from 360 to 80 mg. Thus, the polar species formed as a result of plasma treatment are gradually lost during washing even at R.T.P. Under dyeing conditions, that is washing at 90°C for 30 min, the wettability of the plasma treated PET reaches that of untreated PET fabric (water contact angle=80°) meaning that there is complete loss of all polar species formed by plasma treatment. Surface analysis of plasma treated PET subjected to hot aqueous dyeing conditions shows complete disappearance of the scaly shaped PET surface (Fig. 15b). Only traces or finger prints of the scales remain leaving a smooth surface (Ra = 38 nm). Moreover dyeing of plasma treated PET shows no increase in disperse dye uptake.

3.4 Effect on adhesion of PEG 1500

Atomic Force Microscopy, in the Tapping mode was carried out to better understand the different morphological changes occurring at the PET fabric fiber surface before and after PEG-1500 immobilization with and without a prior plasma treatment of the PET fabric surface. Detailed results have been published elsewhere (Takke, 2010).

Figures 16a and 16b show typical topographical images of a cleaned-untreated PET fiber with and without PEG coating respectively. Though the surface roughness of the PET surface with or without PEG coating is almost the same (~70nm), the untreated PET fiber seem quite smooth and homogeneous. However, after application of PEG, many small thin elliptical and irregular shaped deposits, most probably due to PEG, appear at the fiber surface (see Fig. 16b).

After plasma treatment of PET fiber (at 60 kJ/m²) uniform scale-shaped bumps (6 scales per µm in the x-direction) appear on the PET fiber surface (see Fig. 16c) as a result of surface etching caused by plasma treatment. After immobilizing of PEG 1500, big bumps appear in the foreground relief, covering the regular scaly shaped bumps which can no longer be perceived. However, on the upper part of the image (x =0 to 1), the scaly shaped bumps still appear as if the gaps (valleys) in between scales have not been completely filled with PEG in that region, most probably, because either the PEG does not cover them at all, or only a thin layer of PEG covers the scaly bumps.

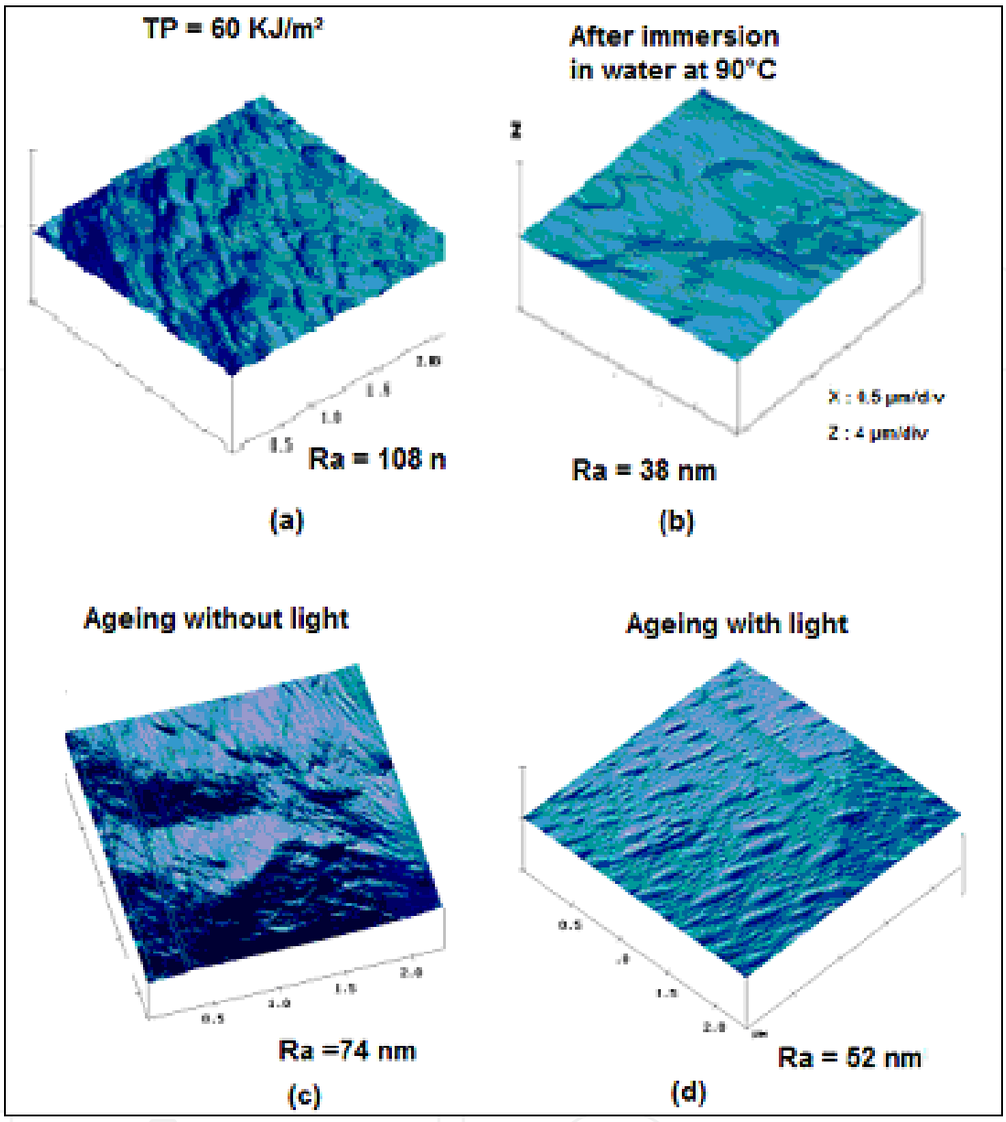

Fig. 15. Tapping mode topographic image of (a) a PET plasma-treated sample at 60 kJ/m², (b) followed by immersion in hot water at 90°C during 30 minutes, (c) after having been subjected to a 20 day-ageing without light and (d) ageing with light

Immobilisation of PEG on both untreated –cleaned PET and plasma treated PET lead to a hydrophilic fabric surface with similar water contact angle (~50°) in both cases. However, wash fastness test carried out at room temperature on PEG coated PET fabrics shows that without plasma treatment there is an increase in water contact angle of the PET fabric with an increase in washing cycles: the hydrophilic PEG molecules adsorbed at the PET surface are gradually desorbed with the washing time. This would mean that only weak cohesive forces exist between the cleaned untreated PET surface and the PEG molecules.

However, a plasma treatment of the PET fabric prior to PEG adsorption improves adhesion between PEG and PET-polyester fabric, since the water contact angle value of the PEG coated fabric remains unchanged with washing time at R.T.P and at 80°C. Therefore, the

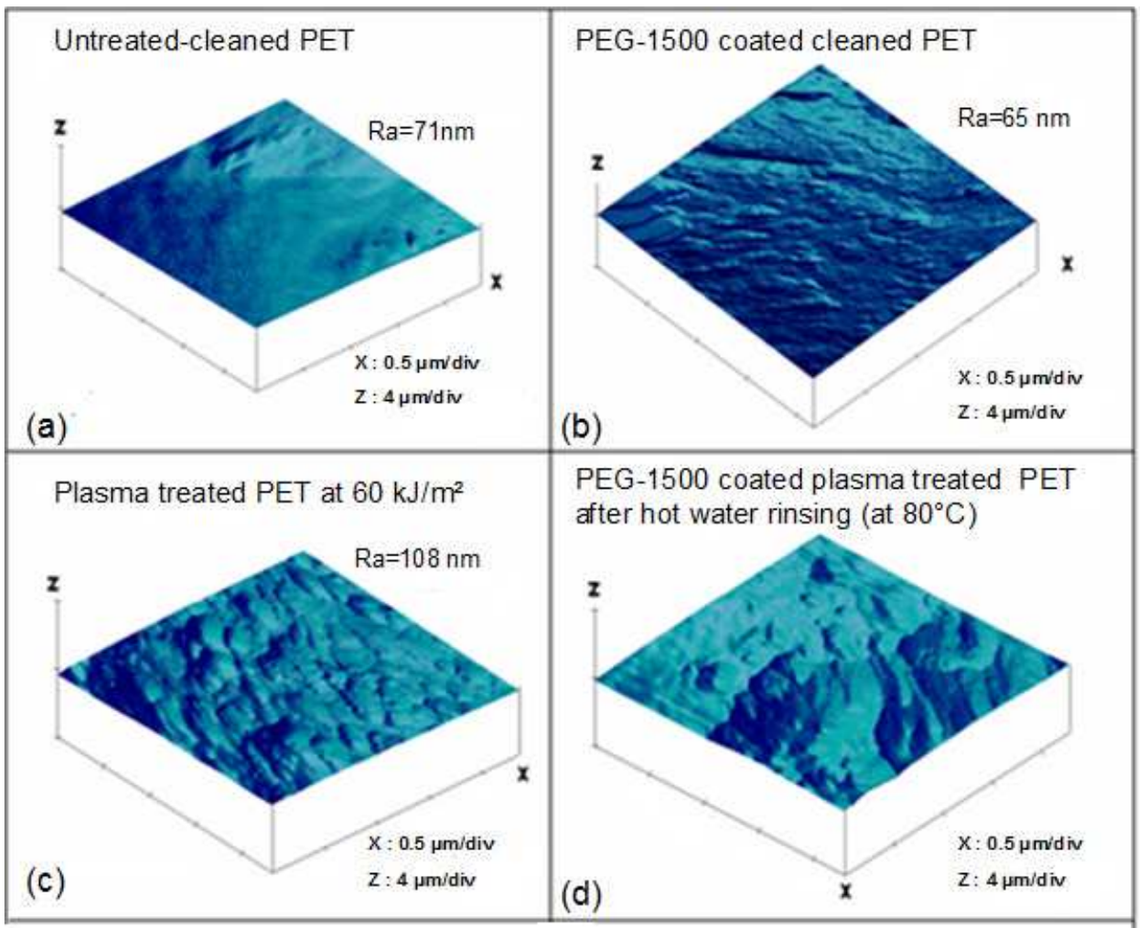

Fig. 16. Tapping Mode AFM Topographical images of (a) an untreated-cleaned PET fiber, (b) a PEG-1500 coated untreated-cleaned PET fiber, (c) a plasma treated PET fiber at 60 KJ/m², (d) a PEG-1500 coated plasma treated PET fiber subjected to wash fastness test at 90°C (Takke, 2011).

PEG molecules are still attached to the plasma treated PET fiber surface and cannot be removed by washing. The chemical or physico-chemical interaction/bonding between the free PEG and the polar species of the plasma treated PET results in an increased adhesion between PEG and PET fabric surface. It is also probable that the increase surface roughness (Ra =108 nm, as shown by AFM images) would enhance this adhesion.

4. Conclusions

AFM seems an invaluable tool to detect all surface morphological modifications taking place during plasma treatment of a PET fabric surface. It confirms that plasma treatment not only adds polarity to the PET surface, but also, depending on the treatment power used, etching of the PET surface by plasma or a reorganisation of the PET surface takes place. AFM also shows the changes that takes place after ageing in presence or in absence of light, and when the plasma treated fabric is subjected to high temperature aqueous conditions. It confirms that the loss of polarity during ageing is also accompanied by morphological changes. AFM

imaging can also be used to obtain the fiber surface topography after the fabric has been padded with a hydrophilic PEG coating and shows the distribution of the coating at the PET fiber surface.

AFM imaging seems to be complementary to the other surface characterisation tools (wettability, XPS) and can be successfully used to characterise textile fiber surface modifications by plasma treatment

5. Acknowledgement

The authors acknowledge Asia Link Project for the realization of this project. We also acknowledge Utexbel for providing us with woven fabric sample used in this work. We would also like to thank Mr. Dassonville, Mr. V. Takke, Dr. F. Leroux, Dr. C. Campagne and Mr. C. Catel for their precious help.

6. References (Part I)

Baselt D.R., Baldeshwielder J.D., "Lateral Force Microscopy of Graphite in air", *J. Vac. Sci. Tech*. B-10 (5), 2316-2322 (Sept/Oct 1992).

Behary, N. et al., "Tribological analysis of glass fibers using atomic force microscopy (AFM)/lateral force microscopy (LFM)", Journal of Applied Polymer Science,75(8), 1013–1025 (2000)

Behary, N. et al., Tribology of Sized Glass Fibers, Part I: Friction Analysis by Lateral Force Microscopy and Electronic Microbalance Technique, *Text. Res. J.*, 78 (8), 700-708 (2000)

Bining, G., Quate, C.F., & Gerber, Ch., "Single-tube three-dimensionnal scanner for scanning microscopy", *Phys. Rev. Lett.* 56, 930 (1986).

Derjaguin, B.V., Muller, V.M., Toporov Yu.P., "Effect of contact deformation on the adhesion of particles" *Colloid Interface Sci*., 53, 314-326 (1975)

Gupta, B.S., "*Frictional Behaviour of Fibrous Materials* ", *Polymer and Fiber Science, Recent Advances*, Edited by Raymond E., Fornes and Richard D. Gilbert, 305-332 (1992)

Gupta, B.S., Wolf, K.W., "Effect of Suture Material and construction on Frictional properties of sutures", *Gynecol. Obster*., 161, 12-16 (1985)

Gupta, S., Molgahzy, E., "Friction in fibrous materials", Part II : Experimental study of effects of structural and Morphological factors", *Text. Res. J.*, 63 (4), 219-230 (1993)

Israelachvili, J., Chen, Y.L, "Fundamental Mechanisms of Interfacial Friction, 1.. Relation between Adhesion and Friction", *J. Phys. Chem*., 97, 4128-4140 (1993).

Johnson, K.L., Kendall, K.,& Roberts, A.D, "Surface energy and contact of elastic solids", *Proc. Roy. Soc. London*, A324, 301-313 (1971)

Marti, O., " Nanotribology : Friction on a Nanometer Scale", *Physica Scripta* T 49, 599-604 (1993).

Meyer, E., and Amer, N.M., "Simultaneous measurement of lateral and normal forces with optical-beam-deflection atomic microscope", *Appl. Phys. Lett*., 57(20), 2089-2090 (1990).

Pashley, M.D., Tabor, D., "Adhesion and micromechanical properties of metal surfaces", *Wear* 100, 7 (1984)

Plueddeman, P., "*Silane Coupling agents*", *Plenum Press, New York* (1982)

R. Overney, and E. Meyer, , "Tribological Investigations using Friction Force Microscopy," *Mrs Bulletin*, 26-34 (May 1993).

Williams J.A., "Engineering tribology" , *Oxford science publications* (1994)

Yamaguchi Y., "Tribology of plastic materials", *Tribology of plastic materials,* Elsevier, Amsterdam (1990)

7. References (Part II)

Borcia G., Anderson C. A. and Brown N. M. D., The surface oxidation of selected polymers using an atmospheric pressure air dielectric barrier discharge. Part I. *Appl. Surface Sci*. 2004, 221, 203

Borcia G., Anderson C. A. and Brown N. M. D., The surface oxidation of selected polymers using an atmospheric pressure air dielectric barrier discharge. Part II, *Appl. Surface Sci*. 2004, 225, 186

Borcia G., Anderson C. A., and. Brown N. M. D, *Plasma Sources Sci*. T." Dielectric barrier discharge for surface treatment: application to selected polymers in film and fiber form . 2003;12:335-344 T

Chatelier, C., Xie, X., Thomas, R., Gengenbach, and Griesser, Hans J., "Effects of plasma modification conditions on surface restructuring", *Langmuir* 1995;11:2585-2591.

Collins M.J., Zeronian S.H., Semmelmeyer M., "The use of aqueous alkaline hydrolysis to reveal the fine structure of poly(ethylene terephthalate) fibers", *J. Appl. Polym. Sci*., 1991, 42, 2149

Fang, Z., Qiu, Y., and Kuffel, E., Formation of hydrophobic coating on glass surface using atmospheric pressure non-thermal plasma in ambient air. *J. Phys. D: Appl. Phys*. 2004; 37:2261-2266.

Haghighatkish M., Youscfi M., "Alkaline hydrolysis of polyester fibers. Structural effects", *Iranian Journal of Polymer Science & Technology*", 1992, 1(2), 56

Harris JM, editor. Poly(ethylene glycol) chemistry: Biotechnical and Biomedical applications (1992), New York: Plenum Press.

Höcker H., Plasma treatment of textile fibers, *Pure Appl. Chem*. 2002, 74(3), 423–427.

Jasso, M., Hudec, I., Alexy, P., Kovacik, D., Krump H., "Grafting of maleic acid on the polyester fibers intiated by plasma atmospheric pressure" *Int. J. adhes. A*dhes. 2006; 26:274-284.

Kailash C. Khulbe,C. Y. Feng,Takeshi Matsuura, Synthetic Polymeric Membranes: Characterization by Atomic Force Microscopy, GERMANY, Springer-Verlag Berlin Heidelberg (2008)

Krump, H., Simor, M., Hudec I., Jasso, M., Luyt A. S., Adhesion strength study between plasma treated polyester fibers and a rubber matrix, *Appl. Surf. Sci*.2005; 240:268-274.

Leroux, F., Perwuelz, A., Campagne C., Behary N., "Atmospheric air plasma treatments of polyester textile structures ", *J. Adhesion Sci. Technol*. 2006;20(9):939-957.

Leroux F., Campagne C., Perwuelz A., Gengembre L., "Fluorocarbon nano-coating of polyester fabrics by atmospheric air plasma with aerosol", *Appl. Surf. Science*, 2008, 254(13), 3902-3908.

Novak, I., Florian S., "Investigation of long-term hydrophobic recovery of plasma modified polypropylene ", *J. Material Sci*. 2004; 39(6) :2033-2036.

Oktem, T., Seventekin, N., Ayhan, H., Piskin E., "Modification of polyester and polyamide fabrics by different in situ plasma polymerization methods", *Turk J Chem*. 2000; 24 : 275-285.Pastore M. and Kiekens P. (2001) In: Surface Characteristics of fibers and textiles, edited by Christopher Pastore, Surfactant Science Series, Vol 9, 298 pages

Takke V., Behary N., Perwuelz A., Campagne C., "Studies on the atmospheric air–plasma treatment of PET (polyethylene terephtalate) woven fabrics": Effect of process parameters and of aging, *J. Appl. Polym. Sci*. 2009, 114(1), 348

Takke V., Behary N., Perwuelz A., Campagne C., Surface and adhesion properties of poly(ethylene glycol) on polyester(polyethylene terephthalate) fabric surface: Effect of air-atmospheric plasma treatment, *J. Appl. Polym. Sci*. 2011, 122 (4), 2621

Verschuren J., Van Herzele P., Clerck, K. De., and Keikens, P, Influence of Fiber Surface Purity on Wicking Properties of Needle-Punched Nonwoven after Oxygen Plasma Treatment, *Text. Res. J.,* 2005; 75(5):437-441.

Vertommen M.A.M.E.,. Nierstrasz V.A, Van der Veer M.,Warmoeskerken M.M.C.G., "Enzymatic surface modification of poly(ethylene terephthalate)", *J. Biotechnol*. 2005, 120, 376

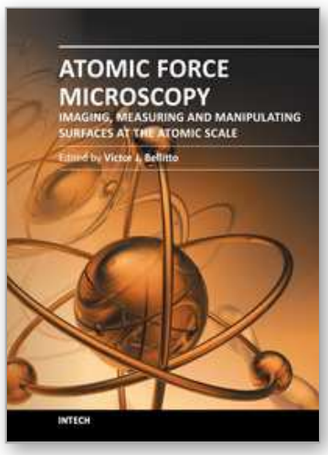

Atomic Force Microscopy - Imaging, Measuring and Manipulating Surfaces at the Atomic Scale

Edited by Dr. Victor Bellitto

ISBN 978-953-51-0414-8
Hard cover, 256 pages
Publisher InTech
Published online 23, March, 2012
Published in print edition March, 2012

With the advent of the atomic force microscope (AFM) came an extremely valuable analytical resource and technique useful for the qualitative and quantitative surface analysis with sub-nanometer resolution. In addition, samples studied with an AFM do not require any special pretreatments that may alter or damage the sample and permits a three dimensional investigation of the surface. This book presents a collection of current research from scientists throughout the world that employ atomic force microscopy in their investigations. The technique has become widely accepted and used in obtaining valuable data in a wide variety of fields. It is impressive to see how, in a short time period since its development in 1986, it has proliferated and found many uses throughout manufacturing, research and development.

InTech Europe
University Campus STeP Ri
Slavka Krautzeka 83/A
51000 Rijeka, Croatia
Phone: +385 (51) 770 447
Fax: +385 (51) 686 166
www.intechopen.com

InTech China
Unit 405, Office Block, Hotel Equatorial Shanghai
No.65, Yan An Road (West), Shanghai, 200040, China
中国上海市延安西路65号上海国际贵都大饭店办公楼405单元
Phone: +86-21-62489820
Fax: +86-21-62489821

IntechOpen